ELSEVIER

Journal of Alloys and Compounds 218 (1995) 197–203

Journal of ALLOYS AND COMPOUNDS

Crystal structure and physical properties of new ternary silicides $R_4T_{13}X_9$ (R, rare earth or uranium; T, rhodium or iridium; X, silicon or germanium)

A. Verniere [a,c], P. Lejay [a], P. Bordet [b], J. Chenavas [b], J.L. Tholence [a], J.X. Boucherle [c], N. Keller [a]

[a] *Centre de Recherche sur les Très Basses Températures, Centre National de la Recherche Scientifique, BP 166, F-38042 Grenoble Cedex 09, France*

[b] *Laboratoire de Cristallographie, Centre National de la Recherche Scientifique, BP 166, F-38042 Grenoble Cedex 09, France*

[c] *CEA Département de Recherche Fondamentale sur la Matière Condensée, SPSMS/MDN, Centre d'Etude Nucléaire de Grenoble, 17 Avenue des Martyrs, F-38054 Grenoble Cedex 09, France*

Received 29 July 1994

Abstract

New ternary silicides have been discovered with the general formula $R_4T_{13}X_9$, where R is a rare earth or uranium, T is rhodium or iridium and X is silicon or germanium. The crystal structure has been solved on a single crystal. The symmetry is orthorhombic with space group *Pnmm*. The lattice constants for $Er_4Ir_{13}Si_9$ are $a = 18.848(3)$ Å, $b = 10.918(2)$ Å and $c = 3.9153(5)$ Å. The formation of the various members of this new family is in competition with that of the well-known ternary silicides RT_3X_2. Their existence as a function of the various elements (rare earth and transition metals) is discussed. The magnetic properties of the iridium-based compounds are presented. All the samples containing a paramagnetic rare earth are magnetically ordered at low temperature. $U_4Ir_{13}Si_9$ and $U_4Ir_{13}Ge_9$ exhibit two ordering transition temperatures: 18 and 6.4. K for the silicide and 25 and 7 K for the germanide.

Keywords: Ternary silicides; Magnetic properties; Germanides

1. Introduction

The ternary silicides and germanides with a rare earth metal and a 3d, 4d or 5d transition element have been extensively studied during the past years. These compounds have numerous crystallographic structure types and interesting physical properties such as mixed valence state, superconductivity coexisting with an antiferromagnetic order and heavy fermion behaviour.

New ternary compounds have been discovered with the general formula $R_4T_{13}X_9$, where R is a rare earth or uranium, T is rhodium or iridium and X is silicon or germanium. The existence of the isotypic members of this new family as a function of the various elements is summarized in Table 1.

It was impossible to prepare both silicides and germanides with Co, Ni and Ru. Of the rhodium-based silicides, only $U_4Rh_{13}Si_9$ could be synthesized, while the germanides of the same series exist for U, Y and all the rare earths from Ce to Lu.

Table 1
Phase stability of $R_4T_{13}X_9$ (A) and RT_3X_2 (B) compounds with R ≡ rare earth, Y, La or U, T ≡ Rh or Ir and X ≡ Si or Ge

	Silicon	Germanium
Rhodium	A: U B: Ce–Lu, Y and La	A: Ce–Lu, Y and U
Iridium	A: Sm–Lu, Y and U B: Ce–Nd	A: Ce–Lu, Y and La

The existence of the $R_4T_{13}X_9$ compounds is correlated with that of the well-known family RT_3X_2 with a $CaCu_5$-related structure type [1]. These two compositions are close in the ternary diagram and the important fact to be noted is that when an $R_4T_{13}X_9$ compound can be prepared, the corresponding RT_3X_2 (with the same elements) does not exist and vice versa (Table 1).

In this paper we report more precisely on the iridium-based silicides in terms of their crystal structure and

SSDI 0925-8388(94)01400-0

magnetic properties. The physical behaviours of the other isotypes will be published later.

2. Sample preparation and crystal growth

The polycrystalline materials have been prepared by direct combination of the high quality elements: 5N rare earth ingots, depleted uranium (resistivity ratio from room to liquid helium temperature, $\rho_{300\,K}/\rho_{4.2\,K}=25$), 4N rhodium and iridium and 6N5 silicon and germanium. Stoichiometric amounts of the starting elements were melted in a water-cooled copper crucible using a high frequency generator under a purified argon atmosphere. To improve the homogeneity, the bulk was turned over and remelted several times. Upon cooling the samples, many tiny $R_4T_{13}X_9$ whiskers can be seen pointing out of the bulk. The typical dimensions of these brittle needle-like single crystals are $20\times20\times200$ μm^3.

The single crystals of $Er_4Ir_{13}Si_9$ and $U_4Ir_{13}Si_9$ used for structural investigations and measurements of the physical properties respectively have been prepared under an inert gas in a tri-arc plasma furnace equipped with a Czochralski puller [2].

After annealing at 900 °C for 8 days under an ultra-high vacuum of 5×10^{-10} Torr, microprobe analysis (Camebax-SX) revealed a pure and homogeneous phase with the right composition.

Furthermore, the samples have been characterized by conventional X-ray diffraction: powder diffractometer, Guinier camera and backscattering Laue technique for single crystals (typically cylinders 3 mm in diameter and 10 mm long).

3. Structure determination of $Er_4Ir_{13}Si_9$ single crystal

The unit cell of $Er_4Ir_{13}Si_9$ was determined by automatic indexing of a Guinier film using Fe $K\alpha_1$ radiation and a silicon internal standard in orthorhombic symmetry. The least-squares-refined cell parameters were $a=18.848(3)$ Å, $b=10.918(2)$ Å and $c=3.9153(5)$ Å.

A small part of a single crystal was ground to a sphere of radius 0.08 mm and mounted on a Philips PW1100 diffractometer equipped with graphite-monochromatized Ag $K\alpha$ radiation; 2793 reflections lying in the sphere of reciprocal space with $\theta\leqslant20°$ and $-4\leqslant l\leqslant1$ were collected in ω scan mode with a 1.5° scan width.

Examination of the reflection intensities indicated that the $0kl, k+l=2n+1$ reflections were absent, leading to the space group *Pnmm*. All data treatments and refinements were carried out using the SDP crystallographic package. The reflections were corrected for Lorentz polarization and spherical absorption effects and averaged in the above space group symmetry, leading to 634 independent reflections with $R_{sym}=4\%$. Direct methods (programme MULTAN) were used to obtain the positions of the heavy atoms (Er, Ir). Subsequent cycles of refinement and difference Fourier synthesis allowed us to determine the positions of all atoms, including Si. Examination of the observed/calculated intensities indicates the presence of strong extinction effects at low angle, so the reflections with $\sin\theta/\lambda\leqslant0.3$ were suppressed from the data. The final refinement cycles were carried out using statistical weights and a $\sigma(I)/I$ cut-off of 3. Positional parameters for all atoms, anisotropic thermal parameters for heavy atoms and isotropic thermal parameters for Si atoms were included. The agreement factors were $R=2.3\%$ and $wR=3.1\%$ with 522 observations and 72 variables. Trying to refine the occupancies on the heavy atom sites led to insignificant deviations from unity, indicating that substitution between Er and Ir sites is very small or absent. Positional and thermal parameters are listed in Tables 2 and 3 respectively and interatomic distances up to 3 Å in Table 4.

Table 2
Atomic coordinates for $Er_4Ir_{13}Si_9$ with space group *Pnmm*

Atom	Position	x	y	z
Er1	4*f*	0.79224(7)	0.0592(1)	$\frac{1}{4}$
Er2	2*b*	0.4804(1)	$\frac{3}{4}$	$\frac{1}{4}$
Er3	2*a*	0.9784(1)	$\frac{1}{4}$	$\frac{1}{4}$
Ir1	4*f*	0.66439(6)	0.0664(1)	$\frac{3}{4}$
Ir2	2*b*	0.85797(9)	$\frac{1}{4}$	$\frac{3}{4}$
Ir3	2*a*	0.65711(9)	$\frac{1}{4}$	$\frac{1}{4}$
Ir4	2*b*	0.22752(9)	$\frac{1}{4}$	$\frac{3}{4}$
Ir5	4*f*	0.46076(6)	0.0607(1)	$\frac{1}{4}$
Ir6	4*f*	0.04654(6)	0.0496(1)	$\frac{3}{4}$
Ir7	4*f*	0.85708(6)	0.8743(1)	$\frac{3}{4}$
Ir8	4*f*	0.64473(6)	0.8777(1)	$\frac{1}{4}$
Si1	2*a*	0.6016(7)	$\frac{3}{4}$	$\frac{3}{4}$
Si2	4*f*	0.5844(4)	0.4304(8)	$\frac{1}{4}$
Si3	4*f*	0.9183(5)	0.0611(9)	$\frac{3}{4}$
Si4	2*b*	0.8975(7)	$\frac{3}{4}$	$\frac{1}{4}$
Si5	4*f*	0.2708(5)	0.3778(8)	$\frac{1}{4}$
Si6	2*b*	0.2666(6)	$\frac{3}{4}$	$\frac{1}{4}$

4. Structure description

The projection of the $R_4Ir_{13}Si_9$ structure along the [001] direction is shown in Fig. 1. The rare earth elements (R) have three different crystallographic sites, but their atomic environments can be described with the same type of distorted polyhedron. All the R atoms are centred inside distorted planar hexagons parallel to the (a, b) plane and separated by a distance equal to the c parameter of the unit cell (3.9153 Å for $Er_4Ir_{13}Si_9$).

Table 3
Thermal parameters for $Er_4Ir_{13}Si_9$ with space group *Pnmm*. U_{ij} are given in Å^2; U_{13} and U_{23} are all zero by symmetry

Atom	U_{11} (B for Si)	U_{22}	U_{33}	U_{12}	B_{eq}
Er1	0.0071(6)	0.0104(6)	0.0052(6)	0.0015(6)	0.597(7)
Er2	0.0073(8)	0.0076(8)	0.0051(9)	0	0.526(7)
Er3	0.0061(8)	0.0085(8)	0.0052(9)	0	0.521(4)
Ir1	0.0041(4)	0.0060(5)	0.0029(5)	0.0000(5)	0.342(3)
Ir2	0.0023(6)	0.0079(7)	0.0195(9)	0	0.781(7)
Ir3	0.0052(7)	0.0058(7)	0.0044(7)	0	0.405(5)
Ir4	0.0024(6)	0.0067(7)	0.0032(8)	0	0.323(8)
Ir5	0.0018(5)	0.0071(5)	0.0042(5)	0.0002(5)	0.344(8)
Ir6	0.0041(4)	0.0076(5)	0.0028(5)	−0.0013(5)	0.381(8)
Ir7	0.0031(4)	0.0061(5)	0.0028(5)	−0.0010(4)	0.315(1)
Ir8	0.0043(4)	0.0055(5)	0.0044(5)	0.0000(5)	0.373(9)
Si1	0.6(2)				
Si2	0.6(1)				
Si3	0.6(1)				
Si4	0.4(2)				
Si5	0.6(1)				
Si6	0.3(2)				

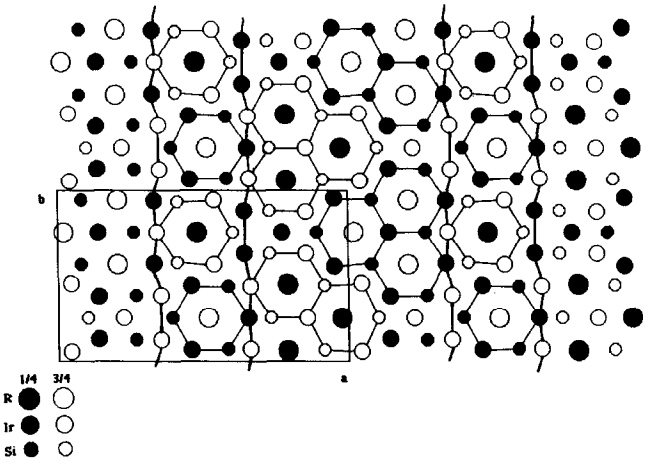

Fig. 1. Projection of $Er_4Ir_{13}Si_9$ structure along the [001] direction.

The transition metal (T) and silicon are alternated in the pseudohexagonal corners. Two types of arrangement of these rare-earth-centred polyhedra can be found:

(1) isolated polyhedra, nearly aligned along the [010] direction, shifted by $c/2$ from one another;

(2) blocks of three different distorted polyhedra with a common vertical face (parallel to the c direction), inside which the three rare earth atoms are on the same layer; they are also shifted by $c/2$ from one another and form zigzag chains along the [010] direction.

All these polyhedra (both isolated and block) are separated by wavy transition metal planes parallel to the c direction. In this structure the silicon atoms are all involved in the various distorted polyhedra, while isolated transition elements can be found.

The iridium and silicon atoms constituting the distorted planar hexagons described before are bonded with interatomic distances (d) shorter than the sum of the respective atomic radii (Σr). These distances are between 2.33 and 2.57 Å when $\Sigma r = 2.679$ Å (for 12-coordinated atoms). The Δ parameter ($\Delta = (d - \Sigma r)/\Sigma r$) generally used to describe the contraction or the expansion of the bonds is equal to −13% and −4% for the shortest and the longest iridium–silicon separation respectively. Such short distances between transition metal and silicon (or germanium) are often reported in the literature for the ternary silicides (or germanides).

The bond lengths between the iridium atoms involved in planar triangles parallel to the (a, b) plane are slightly longer than the sum of the atomic radii ($\Sigma r = 2.72$ Å and $\Delta \approx 2\%$). The shortest distance separating the rare earth atoms is the c parameter of the unit cell, 3.9153 Å.

The lattice constants of the isotypic silicides $R_4Ir_{13}Si_9$ and of $U_4Ir_{13}Ge_9$ are given in Table 5. They were refined from the data obtained with a (Θ–2Θ) gonionmeter using silicon as standard. The a/b ratios for all the compounds are close to $\sqrt{3}$.

5. Structural remarks about the RIr_3Si_2 compounds with R ≡ Ce, Pr and Nd

For samples prepared from the same stoichiometry with the rare earths Ce, Pr and Nd, microprobe analysis revealed multiphase samples without any trace of the "4–13–9" compound. For example, with cerium the analysis revealed the presence of $CeIr_3Si_2$ and $CeIr_2Si_2$ as major and minor parasitic phases respectively. This fact was confirmed by X-ray powder diffraction pattern analysis.

$CeIr_3Si_2$ has been reported to crystallize with a base-centred monoclinic structure ($CeIr_3B_2$-type structure, space group $C2/m$) [3]. The diffraction pattern of a pure $CeIr_3Si_2$ sample, prepared from the right composition and annealed as described above, could not be totally indexed with the published structure. A preliminary structural determination has been carried out with a powder profile refinement using a Rietveld calculation method [4] according to $ErRh_3Si_2$ (space group *Imma*), which is an orthorhombic deformation superstructure of $CeCo_3B_2$ [1].

The data were collected using a Philips PW1050 powder diffractometer with Ni-filtered Cu Kα radiation. The results are listed in Table 6. Fig. 2 represents the measured (circles) and calculated (full line) powder diffraction patterns for $CeIr_3Si_2$ (the difference pattern is shown at the bottom). The final Bragg agreement factor is 8.9% ($R_{profil} = 5.40\%$). This rather bad value is certainly due to a preferred orientation of the powder and the poor quality of the diffraction data. With the

Table 4
Interatomic distances (up to 3 Å) for $Er_4Ir_{13}Si_9$

Ir1–Ir3	2.8057(8) ×2	Ir2–Er3	2.998(2) ×2	Ir3–Ir1	2.8057(8) ×4	Ir4–Ir7	2.866(1) ×4
Ir5	2.736(2)	Si3	2.355(9) ×2	Si2	2.400(9) ×2	Ir8	2.782(2) ×2
Ir8	2.866(1) ×2	Si6	2.35(1)	Si6	2.429(7) ×2	Si4	2.36(1)
Si2	2.472(5) ×2					Si5	2.539(6) ×4
Si5	2.393(9)						
Si6	2.390(6)						
Ir5–Ir1	2.736(2)	Ir6–Ir6	2.843(1) ×2	Ir7–Ir7	2.7131	Ir8–Ir1	2.866(1) ×2
Ir5	2.788(1) ×2	Ir7	2.797(1) ×2	Si3	2.3265	Ir4	2.782(2)
Ir8	2.870(1) ×2	Si3	2.421(9)	Si4	2.4824	Ir5	2.870(1) ×2
Si1	2.378(7)	Si3	2.394(5) ×2	Si5	2.3909	Ir8	2.789(2)
Si2	2.565(6) ×2	Si4	2.429(6)			Si1	2.537(4) ×2
Si2	2.332(8)					Si2	2.384(9)
						Si5	2.523(6) ×2
Si1–Si5	2.78(1)	Si5–Si5	2.79(1)				

Table 5
Lattice constants of isotypic silicides $R_4Ir_{13}Si_9$ and $U_4Ir_{13}Ge_9$

	a (Å)	*b* (Å)	*c* (Å)	*a*/*b*
$Sm_4Ir_{13}Si_9$	18.983	11.016	3.957	1.723
$Gd_4Ir_{13}Si_9$	18.939	10.985	3.947	1.724
$Tb_4Ir_{13}Si_9$	18.908	10.961	3.936	1.725
$Dy_4Ir_{13}Si_9$	18.874	10.943	3.926	1.725
$Ho_4Ir_{13}Si_9$	18.869	10.904	3.917	1.731
$Tm_4Ir_{13}Si_9$	18.832	10.909	3.908	1.726
$Yb_4Ir_{13}Si_9$	18.849	10.916	3.906	1.727
$Lu_4Ir_{13}Si_9$	18.807	10.912	3.899	1.723
$Y_4Ir_{13}Si_9$	18.856	10.922	3.925	1.726
$U_4Ir_{13}Si_9$	18.940	10.926	3.902	1.734
$U_4Ir_{13}Ge_9$	19.361	11.198	3.947	1.729

Table 6
Atomic coordinates for $CeIr_3Si_2$ according to the $ErRh_3Si_2$-type structure with $a=7.1838(2)$ Å, $b=9.7373(3)$ Å and $c=5.6018(2)$ Å

Atom	Position	*x*	*y*	*z*
Ce	4*e*	0	$\frac{1}{4}$	0.7201(5)
Ir1	8*f*	0.2817(2)	0	0
Ir2	4*c*	$\frac{1}{4}$	$\frac{1}{4}$	$\frac{1}{4}$
Si	8*h*	0	0.0749(7)	0.1956(6)

$CeIr_3B_2$-type structural model not all the experimental diffraction peaks could be indexed.

Regarding the X-ray diffraction pattern, $PrIr_3Si_2$ and $NdIr_3Si_2$ are isotypic. Their lattice constants are listed in Table 7. The unit cell volume variation as a function of the rare earth ionic radius confirms the 3+ oxidation state of cerium in this material as reported from magnetic susceptibility measurements as a function of temperature [3]. The $ErRh_3Si_2$-type structure is characterized by distorted silicon hexagons. Si atom pairs are formed with very short interatomic distances corresponding to twice the atomic radius: 2.63 Å for $ErRh_3Si_2$ [1]. From our structural powder refinement of $CeIr_3Si_2$, this distance is already equal to 2.64 Å with one of the bigger rare earth ions, which could explain the disappearance of the "1–3–2" phase for the rare earth elements smaller than Nd.

6. Physical properties of the $R_4Ir_{13}Si_9$ compounds

Magnetic measurements were carried out using a Quantum Design superconducting quantum interference device (SQUID) magnetometer with a superconducting coil ($H \leqslant 5.5$ T) in the 2–300 K temperature range. A.c. susceptibility experiments were performed down to 60 mK using a non-commercial SQUID magnetometer. The materials, $R_4Ir_{13}Si_9$ (R ≡ Sm–Lu, Y and U) and $U_4Ir_{13}Ge_9$, were annealed polycrystalline samples.

All the compounds containing a paramagnetic rare earth follow a Curie–Weiss law at high temperature except for $Sm_4Ir_{13}Si_9$ in accordance with the Van Vleck theory for closely spaced multiplets [5].

The observed effective paramagnetic moments are in good agreement with the theoretical values expected for the rare earth in the 3+ oxidation state. The paramagnetic Curie temperatures Θ_p deduced from the high temperature part of the χ^{-1} (*T*) plots are small and positive for Gd, Dy, Ho and Er and negative for Tb, Yb and U compounds. All these compounds are magnetically ordered at low temperature (up to 6 K). These results are summarized in Table 8.

The magnetization vs. field curve at $T=2$ K for $Gd_4Ir_{13}Si_9$ is shown in Fig. 3. For magnetic fields up to 0.3 T the behaviour is linear and reversible; upon increasing the field, a change in the slope occurs and the magnetization becomes irreversible. The inverse of the molar susceptibility as function of temperature is shown as an inset for a field of 0.2 T.

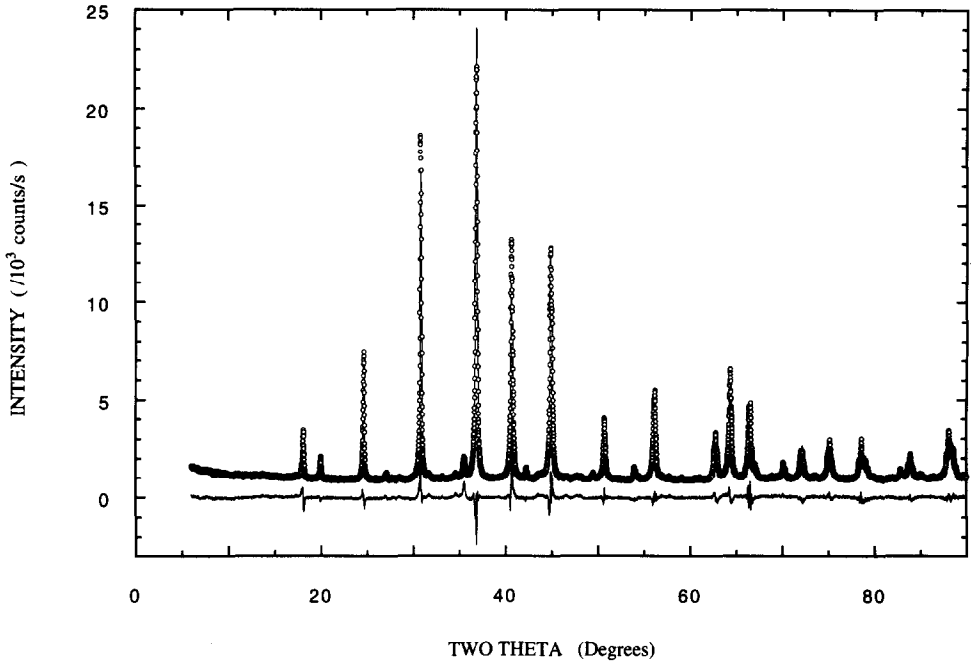

Fig. 2. Measured (circles), calculated (full line) and difference (bottom) powder diffraction patterns for $CeIr_3Si_2$ according to the $ErRh_3Si_2$-type structure (space group *Imma*). $a=7.1838(2)$ Å; $b=9.7373(3)$ Å and $c=5.6018(2)$ Å.

Table 7
Lattice constants of RIr_3Si_2 according to the $ErRh_3Si_2$-type structure

	a (Å)	*b* (Å)	*c* (Å)	*b/c*
$CeIr_3Si_2$	7.1838(2)	9.7373(3)	5.6018(2)	1.738
$PrIr_3Si_2$	7.2073(3)	9.7038(4)	5.5948(2)	1.734
$NdIr_3Si_2$	7.1843(2)	9.6659(3)	5.5817(2)	1.732

$Tb_4Ir_{13}Si_9$ also presents a non-linear magnetization curve at $T=2$ K with two saturations at 0.2 and 1 T respectively (Fig. 4). Neutron powder diffraction at low temperature has been performed on this material to determine its magnetic ordering structure. The results will be published later.

Compared with the rare-earth-based compounds, $U_4Ir_{13}Si_9$ displays a different behaviour. Its magnetic susceptibility measured at 500 Oe does not follow a Curie–Weiss law in any range of temperature (Fig. 5). However, it can be described by an extended law $\chi=\chi_0+C/(T-\Theta_p)$ in a large range of temperature from 300 down to 20 K with $\chi_0=5.07\times10^{-3}$ e.m.u. mol^{-1}, $\mu_{eff}=2.20$ μ_B per U atom and $\Theta_p=-44.4$ K. The fit is shown as an inset in Fig. 5. A Pauli paramagnetic contribution to the susceptibility is also found, for example, in UIr_2Si_2 with a comparable value of the

Table 8
Magnetic data for $R_4Ir_{13}Si_9$ and $U_4Ir_{13}Ge_9$

	Θ_p (K)	μ_{eff} (μ_B per RE^{3+})		Ordering temperature (K)
		Theoretical	Experimental	
$Sm_4Ir_{13}Si_9$	–	1.65 (300 K)	1.47 (300 K)	6.0
$Gd_4Ir_{13}Si_9$	0.19	7.94	8.09	4.5
$Tb_4Ir_{13}Si_9$	−7.57	9.70	9.83	4.3
$Dy_4Ir_{13}Si_9$	1.15	10.63	10.66	4.0
$Ho_4Ir_{13}Si_9$	1.24	10.60	10.22	1.6
$Er_4Ir_{13}Si_9$	1.40	9.59	9.64	2.2
$Yb_4Ir_{13}Si_9$	−6.63	4.54	4.09	0.5
$Lu_4Ir_{13}Si_9$	No superconductivity down to 60 mK			
$Y_4Ir_{13}Si_9$	Superconducting transition at $T_c=70$ mK			
$U_4Ir_{13}Si_9$	−44.40	–	2.20	18 and 6.4
$U_4Ir_{13}Ge_9$	Measured by a.c. susceptibility			25 and 7

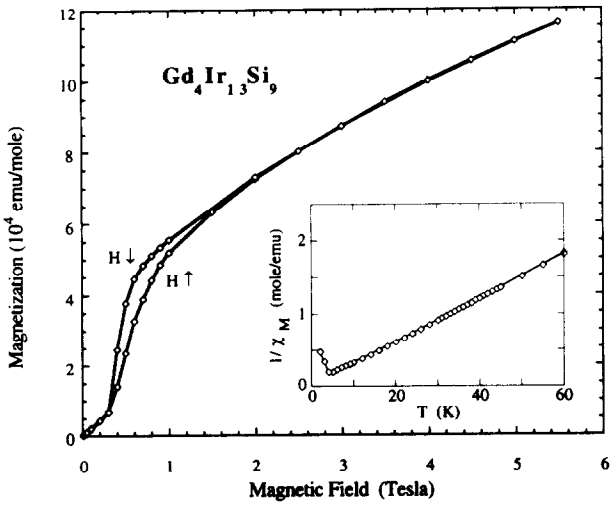

Fig. 3. Magnetization vs. magnetic field up to 5.5 T at $T=2$ K for $Gd_4Ir_{13}Si_9$ ingot. The inverse of the molar susceptibility as function of temperature measured for a field of 0.2 T is shown in the inset (the sample has been cooled down under 500 Oe).

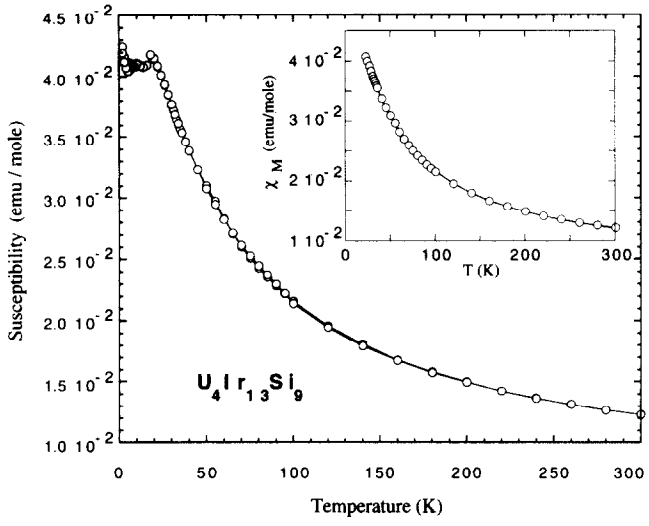

Fig. 5. Molar susceptibility vs. temperature at a magnetic field of 500 Oe for $U_4Ir_{13}Si_9$. The fit of the Curie–Weiss law $\chi=\chi_0+C/(T-\Theta_p)$ from room temperature to 20 K is shown in the inset (the sample has been cooled down under 500 Oe).

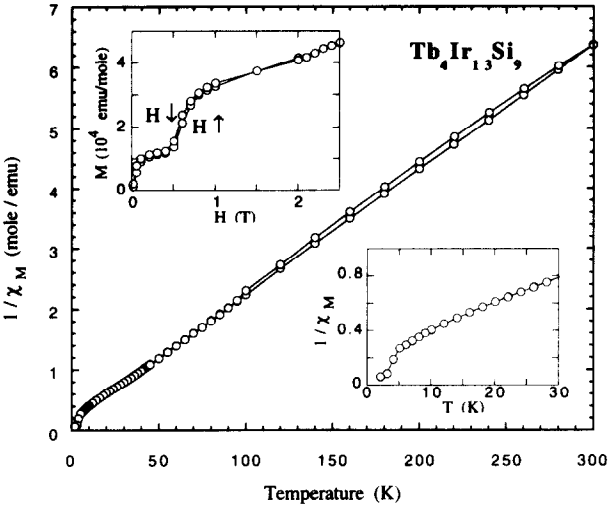

Fig. 4. Inverse of the molar susceptibility vs. temperature at a magnetic field of 500 Oe for $Tb_4Ir_{13}Si_9$ ingot. The magnetization curve at $T=$ 2 K up to 2.5 T is shown in the inset (the sample has been cooled down under 500 Oe).

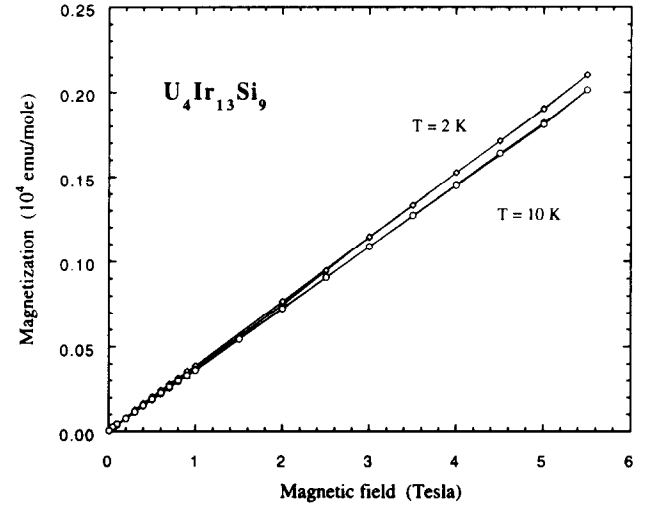

Fig. 6. Magnetization vs. magnetic field up to 5.5 T for $U_4Ir_{13}Si_9$ at $T=2$ and 10 K.

temperature-independent parameter: $\chi_0=1.76\times10^{-3}$ e.m.u. mol^{-1} [6].

The uranium compounds $U_4Ir_{13}Si_9$ and $U_4Ir_{13}Ge_9$ exhibit two ordering transition temperatures: 18 and 6.4 K for the silicide (determined by d.c. susceptibility) and 25 and 7 K for the germanide (determined by a.c. susceptibility). For $U_4Ir_{13}Si_9$ the magnetization vs. field curves at $T=2$ and 10 K stay linear up to 5.5 T (Fig. 6).

These transitions have been confirmed by specific heat measurements. It should be noted that in the ordered state at low temperature $U_4Ir_{13}Si_9$ and $U_4Ir_{13}Ge_9$ have quite large residual electronic specific heat coefficients $\gamma=133$ and 70 mJ mol^{-1} K^{-2} respectively. $U_4Ir_{13}Si_9$ and $U_4Ir_{13}Ge_9$ are new heavy fermion materials presenting a double magnetic transition (to be published). Neutron diffraction experiments are planned on single crystals of $U_4Ir_{13}Si_9$ and $Tb_4Ir_{13}Si_9$ to determine the nature of the magnetic order.

The a.c. susceptibility measurements revealed a very sharp superconducting transition at $T=70$ mK for $Y_4Ir_{13}Si_9$ (Fig. 7). The diamagnetic jump at the transition corresponds to 100% of the sample volume. No superconductivity could be detected for either $U_4Ir_{13}Si_9$ or $Lu_4Ir_{13}Si_9$ down to 60 mK.

7. Note added in proof

Since writing this paper, the crystallographic structure of this new family has been confirmed for the compound

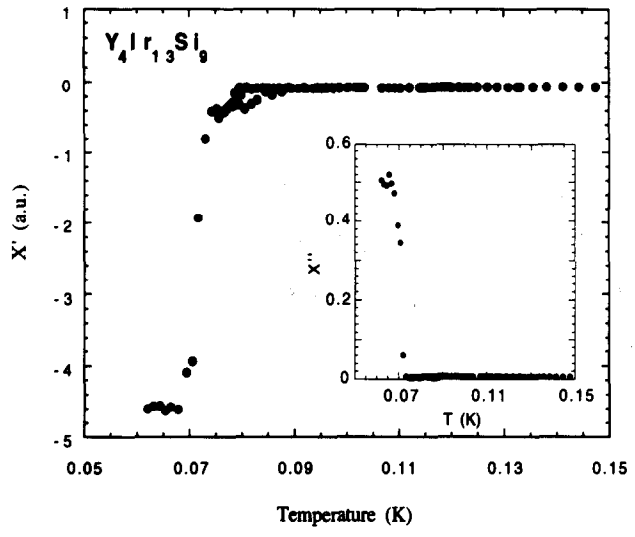

Fig. 7. Superconducting transition of $Y_4Ir_{13}Si_9$ measured by a.c. susceptibility. The imaginary part χ'' of the susceptibility is shown in the inset.

$Ho_4Ir_{13}Ge_9$ by O.I. Bodak et al. (*J. Alloys Comp.*, 202 (1993) 13–15).

Acknowledgements

We wish to acknowledge the help of Mrs. Pierrette Amiot and Georges Battuz with technical support.

References

[1] K. Cenzual, B. Chabot and E. Parthé, *Acta Crystallogr. C, 44* (1988) 221–226.
[2] P. Lejay, J. Muller and R. Argoud, *J. Cryst. Growth, 130* (1993) 238–244.
[3] A.M. Umarji, S.K. Dhar, S.K. Malik and R. Vijayaraghavan, *Phys. Rev. B, 36* (1987).
[4] H.M. Rietveld, *J. Appl. Crystallogr., 2* (1969) 65–71.
[5] J.H. Van Vleck, *The Theory of Electric and Magnetic Susceptibility,* Clarendon, Oxford, 1932.
[6] A.J. Dirkmaat, T. Endstra, E.A. Knetsch, G.J. Nieuwenhuys and J.A. Mydosh, *Phys. Rev. B, 41* (1990) 2589.